Desynchronization of slow oscillations in the basal ganglia during natural sleep

Aviv D. Mizrahi-Kliger[a,1], Alexander Kaplan[b], Zvi Israel[c], and Hagai Bergman[a,b,c]

[a]Department of Neurobiology, Institute of Medical Research Israel-Canada, Hadassah Medical School, The Hebrew University of Jerusalem, 9112001 Jerusalem, Israel; [b]Edmond and Lily Safra Center for Brain Sciences, The Hebrew University of Jerusalem, 9190401 Jerusalem, Israel; and [c]Department of Neurosurgery, Hadassah University Hospital, 9112001 Jerusalem, Israel

Edited by Emery N. Brown, Massachusetts General Hospital, Boston, MA, and approved March 26, 2018 (received for review November 29, 2017)

Slow oscillations of neuronal activity alternating between firing and silence are a hallmark of slow-wave sleep (SWS). These oscillations reflect the default activity present in all mammalian species, and are ubiquitous to anesthesia, brain slice preparations, and neuronal cultures. In all these cases, neuronal firing is highly synchronous within local circuits, suggesting that oscillation–synchronization coupling may be a governing principle of sleep physiology regardless of anatomical connectivity. To investigate whether this principle applies to overall brain organization, we recorded the activity of individual neurons from basal ganglia (BG) structures and the thalamocortical (TC) network over 70 full nights of natural sleep in two vervet monkeys. During SWS, BG neurons manifested slow oscillations (∼0.5 Hz) in firing rate that were as prominent as in the TC network. However, in sharp contrast to any neural substrate explored thus far, the slow oscillations in all BG structures were completely desynchronized between individual neurons. Furthermore, whereas in the TC network single-cell spiking was locked to slow oscillations in the local field potential (LFP), the BG LFP exhibited only weak slow oscillatory activity and failed to entrain nearby cells. We thus show that synchrony is not inherent to slow oscillations, and propose that the BG desynchronization of slow oscillations could stem from its unique anatomy and functional connectivity. Finally, we posit that BG slow-oscillation desynchronization may further the reemergence of slow-oscillation traveling waves from multiple independent origins in the frontal cortex, thus significantly contributing to normal SWS.

sleep | basal ganglia | nonhuman primate | slow oscillations | desynchronization

Sleep is a periodically recurring state of inactivity characterized by loss of consciousness and reduced behavioral responsiveness. Physiologically, sleep is distinguished by global and profound changes in neuromodulation and brain activity (1). Slow-wave sleep (SWS), an essential part of mammalian sleep, is widely viewed as a mediator of homeostatic and learning processes in the brain. Its most evident hallmark is the prevalence of synchronized slow neuronal oscillations (0.1 to 4 Hz) encompassing the macro-, meso-, and microscopic [i.e., EEG, local field potentials (LFPs), and single-neuron action potentials] levels. The cellular basis of these slow oscillations is the rhythmic and synchronized alternation of neurons between up and down states associated with plasma membrane depolarization/hyperpolarization and increased/decreased firing probability, respectively (2). Synchronized slow oscillatory activity has been observed throughout the cortex and thalamus, in the hippocampus, amygdala, and elsewhere (3–7). Slow-oscillation synchronization between different brain regions may confer substantial advantages in information processing and communication during sleep (8). However, synchrony depends on network connectivity (9), and may not be an inherent feature of slow oscillation. Conceivably, alternative schemes where wide-scale slow oscillations are desynchronized may enable multiple independent routes for information transfer in the sleeping brain.

The basal ganglia (BG) are a group of interconnected brain nuclei that receive most of their input and return a significant fraction of their output to the thalamocortical (TC) system (10–12). Intensively studied during waking behavior, the BG are usually associated with action selection, reinforcement learning, and habit formation (13, 14). Rodent studies have suggested that the BG and midbrain dopaminergic neurons play a role in the regulation of sleep–wake behavior (15, 16). However, no systematic work has been conducted to study the BG of nonhuman primates during sleep. Given the major differences between primates and rodents in sleep architecture (17), BG anatomy (18), and physiology (19), we aimed to explore the phenomenology and mechanisms governing sleep in the primate BG and relate them to the wider context of slow oscillations in the brain.

We used multiple (2–8) glass-coated tungsten microelectrodes to record LFP and spiking activity from two young adult female vervet monkeys during 70 full nights of normal uninterrupted sleep. Sleep staging was performed using full polysomnography and video surveillance. We examined the neural activity in the striatum (putamen), pallidum (external and internal segments), subthalamic nucleus, and substantia nigra, as well as the dorsolateral frontal cortex and the ventrolateral tier of the thalamus. Here we first demonstrate that BG neurons change their discharge rate and pattern significantly during the vigilance cycle. We further show that BG neurons exhibit slow oscillations in firing rate during natural SWS, thereby placing the basal ganglia within the wider context of the sleeping brain. Intriguingly, we also demonstrate that the BG maintain a unique state of desynchronization of these slow oscillations. We conclude that slow-oscillation desynchronization is a robust feature of the BG network that persists while most of the brain deepens into concerted and widespread synchronization during sleep.

Significance

Slow-wave sleep is widely associated with synchronized slow oscillations recorded in the cortical mantle and elsewhere in the brain. In this study, we focused on the basal ganglia, a group of interconnected subcortical nuclei implicated in habit learning and in common neurological disorders (e.g., Parkinson's disease). We show that unlike cortical circuits, where slow oscillation is locally synchronized, slow oscillations of firing rates within each basal ganglia nucleus are not phase-locked between adjacent neurons, and are decoupled from the local field potential. Our results establish that neuronal slow oscillations and synchrony do not always co-occur, and highlight decorrelation as a key feature of basal ganglia circuitry that persists even in the most synchronized physiological conditions.

Author contributions: A.D.M.-K. and H.B. designed research; A.D.M.-K., A.K., and Z.I. performed research; A.D.M.-K. analyzed data; and A.D.M.-K. and H.B. wrote the paper.

The authors declare no conflict of interest.

This article is a PNAS Direct Submission.

Data deposition: All data and code are available for downloading from the Basal Ganglia data repository at basalganglia.huji.ac.il/links.htm.

[1]To whom correspondence should be addressed. Email: aviv.mizrahi@mail.huji.ac.il.

This article contains supporting information online at www.pnas.org/lookup/suppl/doi:10.1073/pnas.1720795115/-/DCSupplemental.

Published online April 16, 2018.

Results

To study slow oscillatory activity in the basal ganglia and thalamocortical networks during normal sleep, we recorded spiking and LFP multiple-electrode extracellular activity from the BG and TC networks in sleeping nonhuman primates. The animals were habituated to sleep in a primate chair, with their heads and hands restrained, in a dark sound-attenuating recording chamber. Their vertical sleep posture resembled the one monkeys assume while sleeping in the wild (20) and in our animal facility yard (Fig. S1*A*). We recorded scalp electroencephalogram (EEG) and trapezius electromyogram (EMG) and electrooculogram (EOG) (Fig. S1*B*), and each monkey's face was video-recorded. Sleep staging was semiautomatic and was based on clustering of individual sleep epochs in terms of three features: EEG high/low-frequency range power ratio, EMG root mean square, and eye-open ratio (Fig. 1*A* and *Materials and Methods*). The monkeys' sleep alternated between periods of shallow sleep (N1/2), deep sleep (slow-wave sleep, analogous to N3; *Materials and Methods*), and rapid eye movement (REM) sleep (Fig. 1*B*). The sleep architecture and EEG spectral content during the different stages of the vigilance cycle (Fig. 1*C*) were consistent with results reported for unrestrained nonhuman primates (21) and humans (6). The relative proportions of sleep stages and the average total sleep duration (Fig. S1*C* and Table S1) were similar across recording nights and monkeys.

We recorded the neuronal activity in the dorsolateral frontal cortex, ventrolateral tier of the thalamus, and most of the BG neuronal assemblies (Fig. 1 *D* and *E*). A total of 909 neurons and 1,353 simultaneously recorded neuron pairs met the inclusion criteria (minimal isolation score and discharge rate stability; *Materials and Methods*) and were included in the analysis database (Table S1). All field potentials were recorded simultaneously with well-isolated units to ensure recording location and stability. We recorded from the input (striatum and subthalamic nucleus; STN), central, and output nuclei of the BG (22). In the striatum, we discriminated between phasically active neurons, probably medium spiny neurons (MSNs), which are considered to be the striatal projecting neurons, and tonically active neurons (TANs), which are probably cholinergic interneurons. Here, we focus on the BG projection neurons (Fig. 1*E*; see Fig. S3 for the analysis of TAN activity during sleep). In the STN, central (globus pallidus external part, GPe), and output BG nuclei (globus pallidus internal part, GPi; substantia nigra pars reticulata, SNr), we recorded the high-frequency discharge (HFD) projection neurons, which make up the main neuronal population of these nuclei (23).

BG Neurons Change Their Firing Rates and Patterns During the Vigilance Cycle. In most BG and TC structures, single-neuron firing rates and patterns underwent substantial modulations as the monkey alternated through the vigilance cycle. The firing rate was

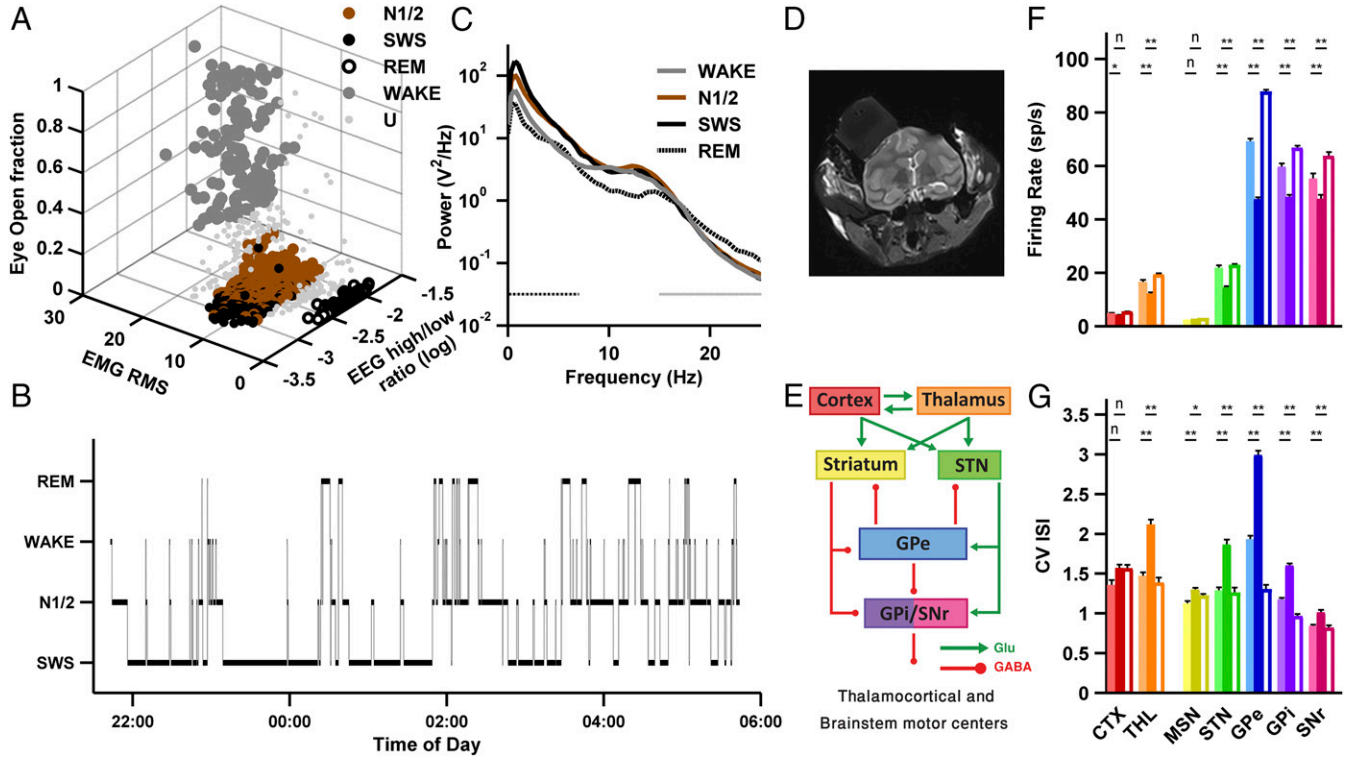

Fig. 1. Polysomnography, electrophysiological targets, and basic discharge features of the basal ganglia and thalamocortical networks. (*A*) A typical example of the output of the semiautomatic sleep staging algorithm for one night (monkey D). The algorithm was used to cluster the different sleep stages (wakefulness, N1/2, SWS, and REM sleep) by high/low EEG power ratio, EMG activity (see also Fig. S2), and eye-open ratio (*Materials and Methods*). (*B*) A typical hypnogram depicting the succession of sleep stages for a single night (monkey D). (*C*) Power spectrum density histogram of EEG activity (C4 electrode) for all epochs of a representative night (monkey N) reveals differences between sleep stages. N1/2 and SWS show increased power in the slow-oscillation range as well as in the spindle (11 to 16 Hz) range. Black dash-dotted and gray dotted horizontal lines indicate the low- (0.1 to 7 Hz) and high- (15 to 25 Hz) frequency ranges, respectively, used for calculating the high/low EEG power ratio. (*D*) A coronal section (~anterior commissure −6 mm) from the post-operative MRI scan showing the brain and the recording chamber (gray box above left hemisphere, monkey N). (*E*) Box and arrow schematic model of the functional anatomy of the TC and BG networks. The color scheme used here is used in all subsequent plots. (*F*) Average firing rate in different brain structures, for wakefulness (light bars), SWS (dark bars), and REM sleep (empty bars). (*G*) Average coefficient of variation (CV) of the distribution of interspike intervals (ISIs) in different brain structures and sleep stages. For *F* and *G*, $n = 66, 96, 72, 94, 321, 175$, and 85 for the cortex, thalamus, MSN, STN, GPe, GPi, and SNr. Horizontal bars indicate statistical comparisons of wakefulness vs. SWS and REM sleep vs. SWS. n, nonsignificant; $*P < 0.05$, $**P < 5 \times 10^{-4}$, Wilcoxon signed-rank test, Bonferroni-corrected. Error bars represent SEM. CTX, cortex; GABA, γ-aminobutyric acid; Glu, glutamate; THL, thalamus; U, unclassified.

significantly lower during SWS than during REM sleep and wakefulness in most structures (Fig. 1*F*). By contrast, the coefficient of variation of the distribution of interspike intervals in most structures was significantly higher during SWS than during REM sleep and wakefulness, indicating a shift to less regular firing (Fig. 1*G*). GPe, GPi, and SNr pauses, spontaneous cessations of firing (24), were most prominent during SWS (Fig. S4).

BG Neurons Exhibit Slow Oscillations in Firing Rate During Slow-Wave Sleep. During SWS, cortical neurons produce oscillations in the range of 0.1 to 4 Hz [slow oscillations (3, 25)] in their firing rate. Here we present evidence for similar slow oscillations in the BG. Fig. 2*A* depicts examples of spiking activity recorded in the dorsolateral frontal cortex and the GPe during wakefulness and SWS, with concurrent cortical depth EEG. The slow oscillatory activity manifested in the TC and BG neuronal firing rate during SWS (Fig. 2*A*, *Lower*) contrasts with the lack of such activity during wakefulness (Fig. 2*A*, *Upper*). This prominent slow oscillatory activity during SWS was also maintained at the population level. Fig. 2*B* presents the single-unit firing rate power spectrum density histograms (normalized by the cumulative power in the 0.1- to 35-Hz range) in the cortex and GPe, representing the TC and BG networks during wakefulness and SWS (light and dark colors, respectively). The spectra were averaged over all 10-s SWS/wakefulness epochs from all recorded cortex or GPe neurons. To quantify the extent to which TC and BG neurons change their firing pattern during SWS, we computed a low-to-high firing rate power ratio (LHPR) by dividing the average relative power at 0.1 to 2 Hz by the average relative power at 9 to 15 Hz (solid and dashed horizontal black lines, respectively, in Fig. 2*B*). A cell was defined as exhibiting slow oscillations in firing rate if its LHPR during SWS was significantly higher than 1 and significantly higher than the median LHPR during REM sleep and wakefulness (*Materials and Methods*). The proportions of cells exhibiting slow oscillations in the cortex and thalamus (50.0 and 47.3%, respectively; Fig. 2*C*)

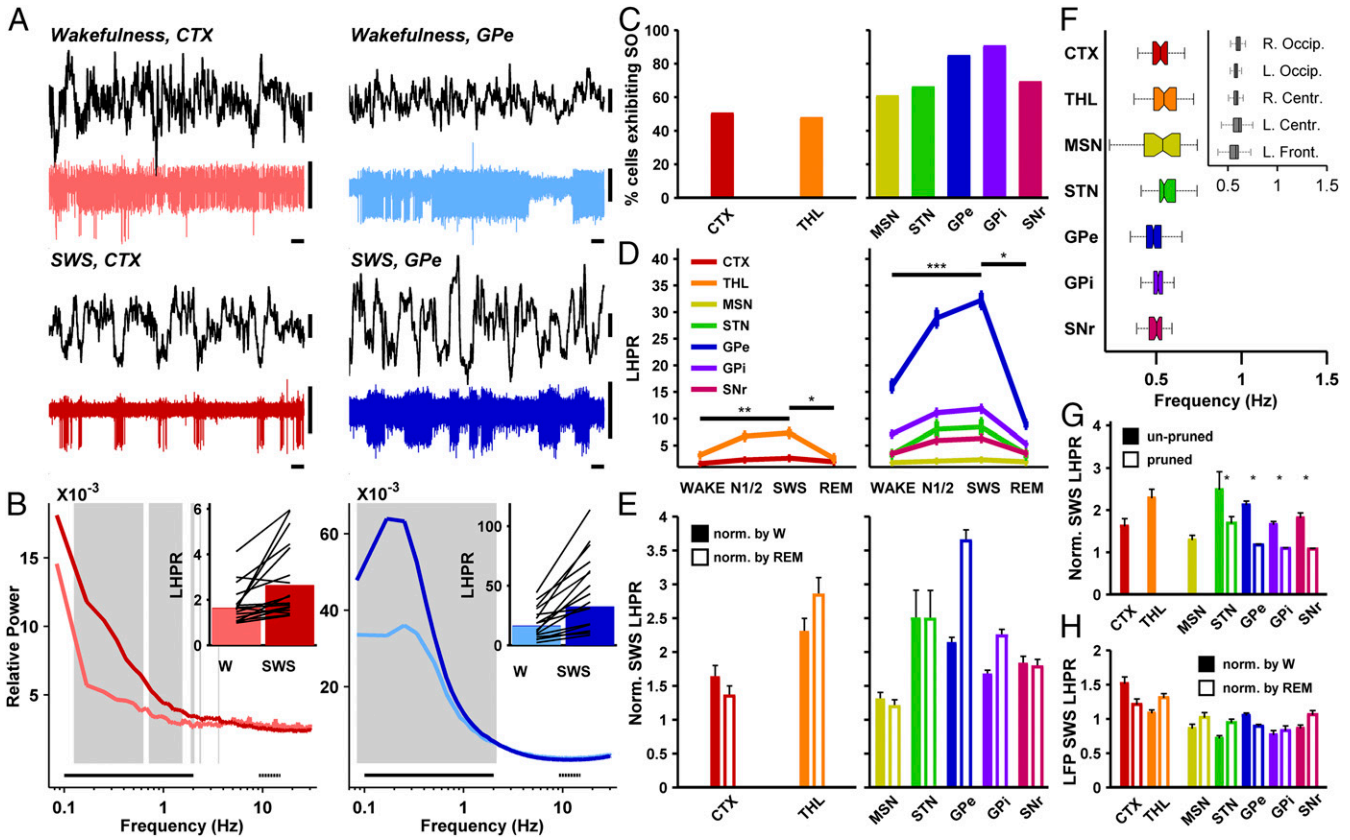

Fig. 2. Slow oscillations in firing rate during SWS in the basal ganglia are at least as prominent as in the thalamocortical network. (*A*) Typical examples of cortical and GPe unit activity during wakefulness and SWS, both recorded simultaneously with cortical-depth EEG (LFP, black). Horizontal bars, 1 s; vertical bars, 100 μV. (*B*) Average relative power spectra of cortical (*Left*) and GPe (*Right*) firing rate during wakefulness (light trace) and SWS (dark trace). Gray background represents frequency ranges where SWS relative power was significantly higher than during wakefulness (Mann–Whitney *U* test, FDR correction for multiple comparisons, $P < 0.05$). (*B*, *Insets*) Low (0.1 to 2 Hz; solid black line in main panel) to high (9 to 15 Hz; dashed black line) power ratios for wakefulness and SWS, across cortical or GPe cells. Bars indicate average LHPR for all neurons, and black lines represent LHPRs for 20 randomly selected neurons. For *B*, *C*, and *H*: $n = 66$, 96, 72, 94, 321, 175, and 85 neurons or LFP recording sites. (*C*) Percent of cells exhibiting slow oscillations in the TC (*Left*) and BG (*Right*) networks during SWS (out of cells recorded during SWS). (*D*) Average LHPRs over all sleep stages in the TC (*Left*) and BG (*Right*) networks, for cells exhibiting slow oscillations. For *D*–*G*: $n = 27$, 43, 41, 61, 257, 154, and 57 neurons. $^{*}P < 0.05$, $^{**}P < 0.001$, $^{***}P < 10^{-5}$. SWS vs. N1/2: $P < 0.05$ for MSN, GPe, GPi, and SNr; others nonsignificant, Wilcoxon signed-rank test, Bonferroni-corrected. (*E*) Average LHPRs for the TC and BG, during SWS, normalized by either mean wakefulness LHPR (filled bars) or mean REM LHPR (empty bars). Wakefulness normalization: All comparisons were nonsignificant except thalamus vs. MSN, $P < 5 \times 10^{-3}$. REM normalization: cortex vs. GPe, GPi, and SNr, $P < 0.05$; thalamus vs. MSN and SNr, $P < 5 \times 10^{-5}$. All other comparisons were nonsignificant. Mann–Whitney *U* test, Bonferroni-corrected. (*F*) SWS slow-oscillation frequency per structure. (*F*, *Inset*) EEG slow-oscillation frequency. (*G*) SWS LHPRs (normalized by mean wakefulness LHPR) before and after random spike pruning of BG high-frequency discharge neurons (Fig. S6). Before vs. after pruning, $P < 0.05$ for all four structures, Wilcoxon signed-rank test, Bonferroni-corrected. $^{*}P < 5 \times 10^{-4}$, Wilcoxon signed-rank test, power ratio vs. 1. (*H*) LFP SWS LHPRs, normalized by mean wakefulness LHPR (filled bars) or by mean REM LHPR (empty bars) for all recording sites in the TC and BG networks. Wakefulness-normalized LFP LHPR was higher than 1 for the cortex ($P < 5 \times 10^{-5}$) and lower than 1 ($P < 5 \times 10^{-3}$) for all BG structures except the GPe (Wilcoxon signed-rank test, Bonferroni-corrected). REM sleep normalization of LFP LHPRs yielded similar results. Error bars represent SEM. SO, slow oscillations; W, wakefulness.

were in line with those reported for these structures during normal sleep and anesthesia (4, 6). All of the BG neuronal assemblies displayed higher percentages of cells exhibiting slow oscillations than in the TC network (60.3 to 90.1%; Fig. 2*C*). In what follows, the firing rate LHPRs are only discussed for those TC and BG cells exhibiting slow oscillations (Table S1, numbers in parentheses). Average LHPRs in the TC and BG structures, for all sleep stages, are shown in Fig. 2*D*. LHPRs were consistently higher during SWS (when the EEG exhibits slow oscillations) than during wakefulness or REM sleep. Further, in most structures, SWS LHPRs were also significantly higher than N1/2 LHPRs. The LHPRs differed not only between sleep stages but also between brain structures, partly due to differences in firing rates (see below). To enable interstructure comparison, we normalized the LHPRs calculated during SWS by the mean LHPR calculated during wakefulness (Fig. 2*E*, filled bars) or during REM sleep (Fig. 2*E*, empty bars). Wakefulness-normalized SWS LHPRs were not significantly different in TC compared with BG neurons, apart from the MSN LHPR, which was lower than the thalamus LHPR. REM-normalized SWS LHPRs were significantly higher for GPe, GPi, and SNr than for the cortex, and higher for the thalamus than for MSN and SNr (Fig. S5 shows normalized SWS LHPRs for all stages and structures).

TC and BG slow oscillations during SWS were also similar in their mean frequency: For the cortex and thalamus, the mean frequencies were 0.51 and 0.55 Hz, whereas the BG mean frequencies ranged from 0.49 to 0.57 Hz (Fig. 2*F*). These frequencies were also similar to the EEG slow-oscillation frequency during SWS (Fig. 2*F*, *Inset*).

BG Slow Oscillations Are Not Abolished by Random Spike Pruning. Despite the normalization of the SWS LHPR by its wakefulness or REM values (Fig. 2*E* and Fig. S5), it could still be argued that the abundance of slow oscillations in the BG HFD neurons is simply a consequence of their higher firing rate (26). To examine this hypothesis directly, we performed random spike pruning such that each cell's pruned mean firing rate was as low as four spikes/s, similar to the average cortical firing rate during SWS. Pruning significantly reduced BG HFD neurons' wakefulness-normalized LHPR, but the pruned LHPR was still significantly higher than 1 (Fig. 2*G*). These results suggest that SWS slow oscillations in firing rate are a fundamental characteristic of the BG network, and that the intrinsic high discharge rates of HFD neurons allow BG slow oscillation to become even more prominent. Fig. S6 shows that HFD neurons' slow oscillations are preserved as well when spikes are pruned to the lower firing rate of two spikes/s characteristic of MSN firing.

Unlike Unit Activity, LFP Slow Oscillatory Activity Is Markedly Lower in the BG than in the Thalamocortical Network. Finally, we wished to examine whether BG slow oscillations were also present in the LFP (Fig. 2*H*). We found that contrary to unit activity, LFP slow oscillations were dramatically reduced in the BG compared with the TC network. Average wakefulness-normalized SWS LHPRs (Fig. 2*H*, filled bars) were significantly higher than 1 for the cortex but lower than 1 for BG structures. REM sleep normalization of SWS LHPRs yielded similar results (Fig. 2*H*, empty bars).

Considered collectively, our results demonstrate that during the "synchronized" brain state (SWS), but not during the "activated" brain states (REM sleep and wakefulness), BG nuclei manifest slow oscillations in firing rate comparable to those characteristic of the TC network, or even stronger. These slow oscillations are prominent at the BG single-cell spiking level and weaker in the BG local field potential.

Contrary to the Thalamocortical Network, BG Pairwise Firing Is Not Correlated During SWS. The manifestation of BG slow oscillations during natural SWS might suggest that, similar to EEG (3) and TC neuronal activity (9, 27), BG neurons should also be highly correlated during SWS. However, spike-to-spike cross-correlation analysis of pairs of simultaneously recorded BG neurons across vigilance stages revealed that they remained uncorrelated even during SWS. Fig. 3*A* depicts examples of simultaneously recorded cortex and GPe cells during wakefulness and SWS. During SWS, both cortical and GPe cells exhibited slow oscillations in firing rate. In the cortex, spiking was synchronized between cells and locked to the troughs of the concurrent-depth EEG oscillation, whereas in the GPe spiking was neither synchronized between cells nor locked to the cortical-depth EEG. Fig. 3 *B* and *C* show the average spike-to-spike cross-correlation histograms for the TC (*Left*) and BG (*Right*) cell pairs during wakefulness and SWS, respectively. During both wakefulness and SWS, cortical and thalamic cells tended to fire action potentials simultaneously. In sharp contrast, the majority of pairs in the BG maintained uncorrelated firing.

To obtain a quantitative representation of these differing tendencies for correlated firing, we calculated the area under the curve of the cross-correlation histograms. This area was significantly higher for the TC group than for the BG group in all vigilance states (Fig. 3*D*). Thus, the spike-to-spike correlation analysis showed that during the synchronized state of the vigilance cycle (SWS), as during the activated states (REM and wakefulness), correlated activity remained absent in the BG. On the other hand, spike pairwise correlations were present in the TC network during both SWS and the activated states. A cross-correlation analysis solely over pairs of cells exhibiting slow oscillations yielded similar results.

Contrary to the Thalamocortical Network, BG Slow Oscillations Are Desynchronized Between Cells. To recapitulate, most BG neurons manifested slow oscillations in firing rate during SWS, to an extent that was at least comparable to the cortex and thalamus (Fig. 2). However, they did not exhibit the spike-to-spike correlations characteristic of cortical and thalamic neuronal pairs (Fig. 3). This apparent discrepancy may be resolved by considering the possibility that individual slow waves in the BG may not be phase-locked (e.g., Fig. 3*A*, *Right Lower*).

To test this hypothesis, we examined the phase locking and correlations of single slow-oscillation waveforms in pairs of cells exhibiting slow oscillations in the TC and BG. Fig. 4*A* presents circular distribution histograms of the phase differences between peaks of slow waves in simultaneously recorded pairs of cells within the TC and BG networks. In the cortex and thalamus (Fig. 4*A*, *Left*), slow-oscillation wave peaks were preferably aligned together, as evidenced by the abundance of phase differences around zero. By contrast, BG slow-oscillation peaks (Fig. 4*A*, *Right*) were not aligned. This difference between the TC and the BG networks was also evident in the average values of the phase-lock indices of the distributions of phase differences (PLIs; Fig. 4*B*). PLI values range from 0 (where phases distribute evenly around the circle) to 1 (all phase vectors point in the same direction). Cortex and thalamus PLIs were higher than all BG PLIs (Fig. 4*B*), indicating a greater concentration of phase vectors pointing in the same direction.

Recent publications (28) have emphasized the importance of the shape of periodic waveforms. We therefore calculated the correlation between single slow waves of neuron pairs in the BG and TC networks. Fig. 4*C* shows that single slow-oscillation waveforms in the TC network exhibited a tendency toward higher positive correlations, whereas in the BG network the distribution of correlation coefficients was roughly flat. The average correlation coefficients were significantly higher for the TC waveforms (Fig. 4*D*).

One possible explanation for these results is that the typical distances (0.5 to 3 mm) between our simultaneously recorded neurons may have been functionally shorter in the TC than in the BG network. Specifically, rather than complete desynchronization, closer BG cells may in fact have been synchronized and synchrony weakened with distance. In this scenario, a positive correlation would be expected between intercell distance and phase difference. However, in our data, the phase synchrony (in the TC) or lack thereof (in the BG) was not related to distance (Pearson's r in the range of −0.103 to 0.039 for all TC and BG pairs, and the effect size, measured by Cohen's d, was correspondingly low, ranging from −0.207 to 0.078; Fig. 4*B*, *Inset*). These results suggest

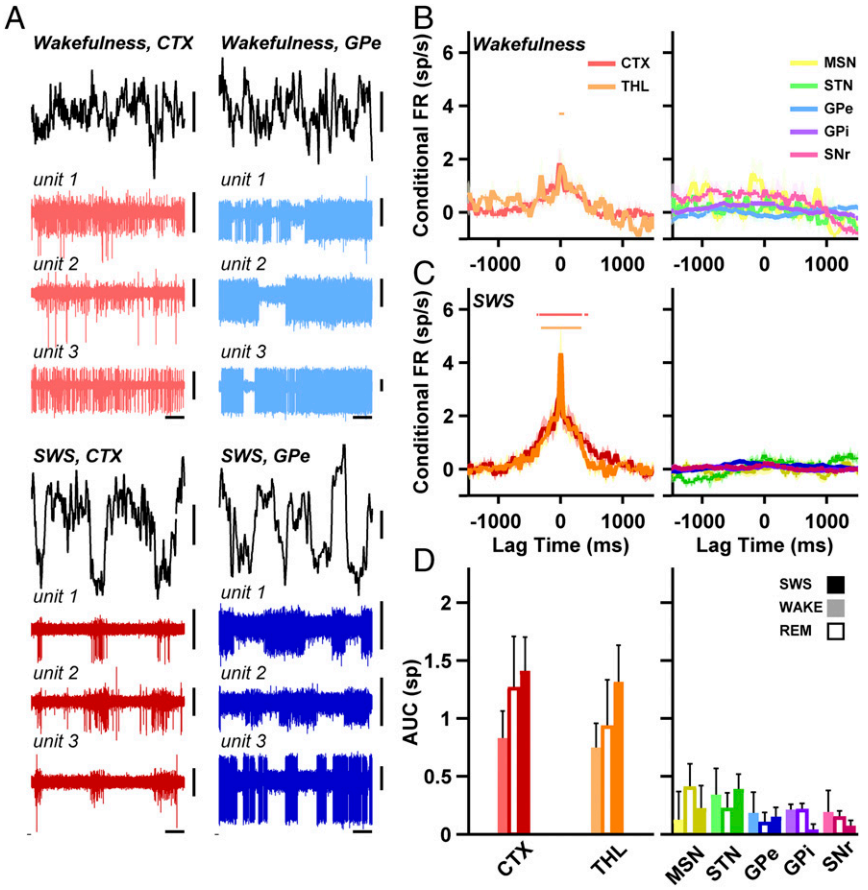

Fig. 3. Unlike the thalamus and cortex, spike-to-spike correlations in the basal ganglia are absent even during SWS. (*A*) Typical examples of multielectrode simultaneous recording of three neurons in the TC and BG networks during wakefulness and SWS (units 1 to 3 in *Upper* and *Lower* are not the same). Horizontal bars, 1 s; vertical bars, 100 μV. (*B*) Average spike-to-spike correlation histograms in the TC (*Left*) and BG (*Right*) networks during wakefulness. The firing rate was smoothed and normalized such that the mean background firing was 0 for all nuclei. Colored horizontal lines represent delays where the cross-correlogram was significantly higher than one spike per s. Numbers of pairs: n = 34, 89, 17, 41, 496, 348, and 60 for the seven structures. Wilcoxon signed-rank test, FDR-corrected for multiple comparisons, $P < 0.05$. (*C*) Same as *B*, only for SWS (n = 42, 114, 23, 55, 575, 404, and 73 pairs). (*D*) Area under the curve (AUC) for 1,500 ms around the trigger spike in the cross-correlation histograms. Light, empty, and dark bars are for wakefulness, REM, and SWS (wakefulness and SWS numbers of pairs as in *B* and *C*; REM numbers of pairs: n = 19, 47, 7, 27, 347, 281, and 46). AUC for TC group vs. BG group, one-way ANOVA, planned contrasts; SWS: df = (6, 1,280), $P < 5 \times 10^{-6}$; wakefulness: df = (6, 1,079), $P < 5 \times 10^{-4}$; REM: df = (6, 768), $P < 5 \times 10^{-3}$. Continuous shading around the traces in *B* and *C* and error bars in *D* represent SEM. FR, firing rate.

that the BG slow-oscillation desynchronization was not distance-related. Similarly, we investigated the possibility that the phase difference might be related to a similarity in frequency (i.e., cells that oscillate in closer average frequencies would tend to be more synchronized) and found negative results (Pearson's r in the range of −0.083 to 0.021, and Cohen's d in the range of −0.166 to 0.041 for all TC and BG pairs).

Unlike the Cortex and Thalamus, BG Spiking Is Decoupled from LFP During SWS. We have shown that the BG LFP (recorded from microelectrode tips relative to skull screw reference; Fig. 2*H*) exhibited a significantly lower degree of slow oscillation compared with the cortex. Next, we analyzed the phase locking between spiking and LFP activities in TC and BG neurons that exhibited slow oscillation (Fig. 4 *E* and *F*). The cortical and thalamic firing tended to concentrate around the trough of the LFP oscillation (Figs. 3*A* and 4*E*, *Left*), whereas in the BG no preferred LFP slow-oscillation phase was apparent for spiking (Fig. 4*E*, *Right*). We computed the PLI for the distribution of LFP slow-oscillation phases in which spikes occurred. Here as well the average PLI was significantly higher for cortical cells than for BG (Fig. 4*F*) and higher for thalamic cells than for the GPe, GPi, and SNr. Correlation analysis of the LFP recorded by neighboring monopolar electrodes yielded similar results: The LFP signal, filtered to contain only energy in the slow-oscillation frequency domain (0.1 to 2 Hz), was more correlated between electrodes in the TC than in the BG network [TC average correlation, 0.60; BG average correlation, 0.37; one-way ANOVA, planned contrasts; degrees of freedom (df) = (6, 823), $P < 5 \times 10^{-5}$].

Taken together, our data support the idea that both TC and BG neurons exhibit slow oscillations in firing rate during SWS. However, whereas the TC network is hallmarked by a state of single-neuron and EEG/LFP slow-oscillation synchronization, in the BG slow oscillation is desynchronized between neurons, regardless of the distance between them, and decoupled from the EEG and LFP.

Discussion

The finding that basal ganglia neurons exhibit slow oscillations (~0.5 Hz) in firing rate places the BG in the broader scheme of the sleeping brain. In contrast, BG slow-oscillation desynchronization, which persists even through the most naturally synchronized brain state of slow-wave sleep, singles them out as a unique exception in the central nervous system (3–7).

Changes in GPe discharge rate or pattern during sleep or eye closure have been reported in monkeys (29, 30), but these observations were limited and lacked a firm basis of polysomnography-based sleep staging. Rodent studies reported SWS 1- to 2-Hz bursting in the STN (31) and rhythmic membrane potential changes in MSNs correlated with cortical EEG (32). Bursty firing during sleep (using only EEG for staging) was also observed intraoperatively in 11 STN neurons in Parkinson's disease patients (33). Finally, slow membrane potential oscillations in MSNs and slow oscillations in STN and GPe firing rates were reported during anesthesia in rats (34–37). These results provide evidence for the ability of the BG neural substrates to maintain slow oscillations given a correlated low-frequency cortical input.

Slow Oscillation in the BG May Originate in the TC Network. Sleep slow oscillations are believed to initiate in the cortex and propagate to other brain structures (6, 27). This is suggestive that slow oscillations observed in the BG may originate in the TC. The BG receive significant input from the TC network through the STN and striatum (10–12), and exhibit stronger slow oscillations during SWS than during other vigilance states (Fig. 2*D* and Fig. S5). Furthermore, the BG slow-oscillation frequency is comparable to TC or EEG frequencies (Fig. 2*F*). In anesthetized rats, low-frequency rhythmic oscillation in BG neurons (STN, GPe,

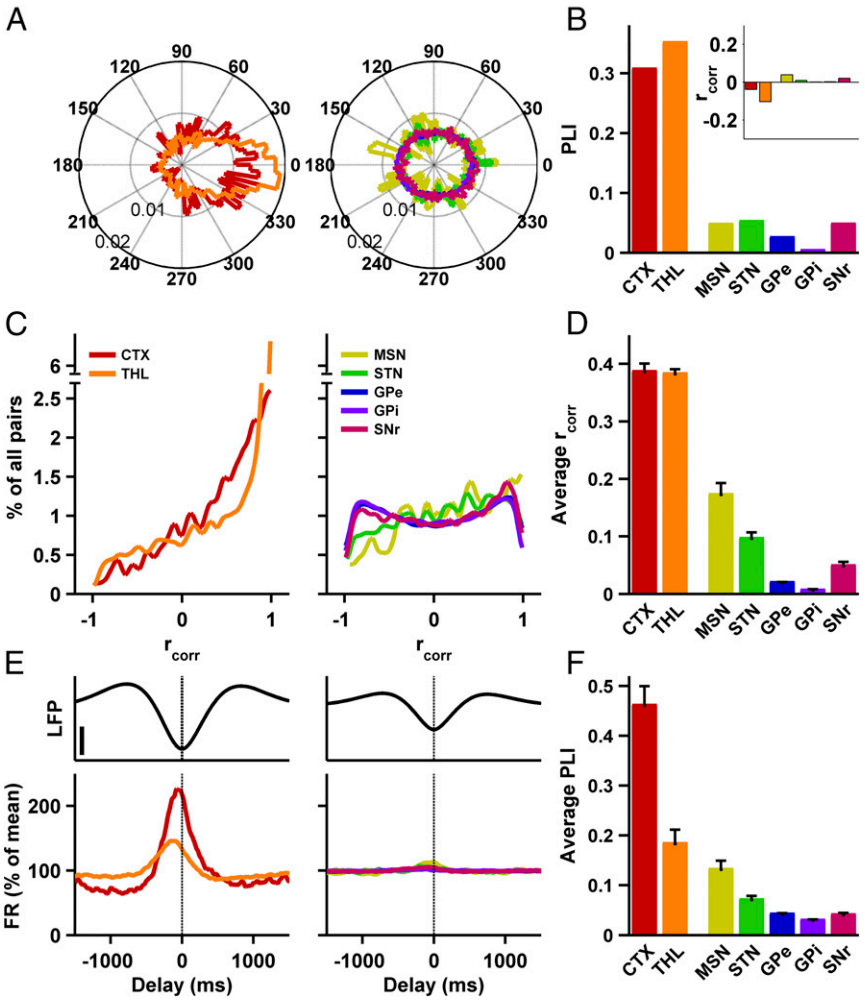

Fig. 4. Slow oscillations in the basal ganglia are desynchronized between cells and decoupled from the LFP. (*A*) Polar histograms of phase differences between slow-oscillation peaks of simultaneously recorded cells in the TC (*Left*) and BG (*Right*) networks. Circle radii, marked on circles, indicate relative proportions of phases in 4.8° bins (n = 565, 4,916, 699, 2,593, 170,098, 98,942, and 7,875 slow-wave pairs, for the seven structures, for all data in *A*–*D*). (*B*) Phase-lock index for the distribution of phase differences. Thalamus or cortex vs. each of the BG structures, two-group concentration homogeneity test, $P < 5 \times 10^{-14}$, Bonferroni-corrected. (*B*, *Inset*) Pearson correlation coefficients of the correlation between phase difference and intercell distance, for all BG and TC structures. (*C*) Distribution of Pearson correlation coefficients between concurrent slow-oscillation waveforms. Note the break of the y axis for the thalamus trace (*Left*). (*D*) Mean population Pearson correlation coefficient. Mann–Whitney U test, thalamus or cortex vs. each of the BG structures, $P < 5 \times 10^{-17}$, Bonferroni-corrected. (*E*) Unit discharge rate around the trough of concurrent LFP slow oscillation in TC (*Left*) and BG (*Right*) neurons exhibiting slow oscillations (smoothed and averaged across units). (*E*, *Upper*) Average traces of LFP slow oscillation. Vertical bar, 50 μV. Firing rate for every unit is calculated as the percent of the average firing rate of the unit. For *E* and *F*: n = 27, 43, 41, 61, 257, 154, and 57 neurons for the seven structures. (*F*) PLI of the distribution of single-spike phases in relation to the concurrent LFP slow oscillation, for all structures, averaged across cells. Mann–Whitney U test, cortex vs. each of the BG structures, $P < 1 \times 10^{-7}$, Bonferroni-corrected. Thalamus vs. GPe, GPi, and SNr, $P < 5 \times 10^{-4}$; thalamus vs. MSN and STN, non-significant, Bonferroni-corrected. Error bars in *D* and *F* represent SEM.

MSNs) was disrupted by electric stimulation to the cortex resulting in loss of cortical synchronization, thus supporting the claim for the cortical origin for BG slow oscillation (35, 36).

The ascending reticular activating system, widely assigned a critical role in the cortical transition to SWS (38), may also play a role in the entrainment of BG nuclei into slow oscillation, presumably through the thalamic intralaminar nuclei and histaminergic, serotonergic, and cholinergic BG innervation (39, 40). Intriguingly, the dopaminergic substantia nigra pars compacta (SNc) neurons did not exhibit firing rate modulation during SWS (41, 42). These results are strengthened by our finding of a lack of firing rate modulation of striatal cholinergic interneurons (TANs) as a function of vigilance state (Fig. S3). By contrast, ventral tegmental area neurons, which probably innervate the ventral striatum and frontal cortex, have recently been shown to be involved in the regulation of the sleep–wake cycle in rodents (16).

In the work cited above, reporting no changes in firing rate during the vigilance cycle in SNc dopaminergic neurons, firing rate oscillations and between-cell correlations were not evaluated. Such sleep-related modulation of firing rate oscillations or neuronal correlations in the SNc, rather than mere changes of firing rate, may indeed play a role in the emergence of the BG neuronal activity modulations shown above. Indeed, a possible role for SNc dopaminergic neurons in sleep regulation is suggested by the stimulating effects of dopaminergic agents (43) and by recent work showing that SNc lesions in rats and primates resulted in a substantial reduction of NREM/SWS time and a fragmentation of sleep–wake states (44, 45). Alternatively, a recent study (46) suggested that axonal dopamine release might be substantially affected by the concurrent state of nicotinic acetylcholine receptors, which could possibly override the lack of changes in the firing rate and pattern of the dopaminergic neurons.

Possible Mechanisms for the Desynchronization of BG Slow Oscillations. Attributing a thalamocortical origin to BG slow oscillations does not account for slow-oscillation desynchronization in the BG. The lack of spike-to-spike correlations in BG HFD neurons is not unique to sleep, and was originally reported in awake monkeys (47). Thus, uncorrelated firing is conceivably an underlying feature of the healthy BG, and may stem from its normal anatomy and physiology. At least two nonmutually exclusive mechanisms may account for the emergence of desynchronized BG activity: active desynchronization by lateral inhibition (48, 49), or an anatomical pattern of parallel segregated hardwiring that guarantees that different BG cells only share a minor fraction of their input (50). These are discussed in detail below.

Lateral inhibition. BG GABAergic neurons (MSNs and GPe, GPi, and SNr neurons) project onto neighboring cells' somata and dendrites (51). Given the high spontaneous firing rates of the GPe, GPi, and SNr neurons and the high anatomical density of MSN collaterals, these cells may exert powerful inhibition on their neighbors. This mode of lateral inhibition has been suggested to be a potent active decorrelation mechanism (49). A state of massive lateral inhibition in BG nuclei is likely to manifest in pairs of simultaneously recorded cells exhibiting a negative correlation or a winner-take-all dynamic (52). We observed a small percentage of BG cells showing nonflat cross-correlations, but these pairs exhibited both facilitation and inhibition (53).

However, the lack of strong negative BG correlations cannot exclude milder states of active decorrelation [e.g., the "winners-share-all" mechanism (48)], especially in the striatum. In any case, the lateral inhibition mechanism does not explain the lack of pairwise correlations in the STN, which is composed almost entirely of excitatory (glutamatergic) projection neurons. Thus, functionally strong lateral inhibition is probably not the major mechanism of BG desynchronization.

Sparse common inputs. The highly convergent BG neuronal input from the cortex and thalamus converges even further through the BG neuronal assemblies, as evidenced by the sharp decrease in tissue volumes and cell numbers down this axis (10, 54, 55). Anatomical tracing studies have shown that a single GPe or GPi/SNr cell samples the activity of numerous striatal cells, any one of which samples numerous cortical/thalamic cells (10, 12, 55, 56).

Recent work has suggested that rather than being synchronized across the cortical mantle, individual cortical slow waves are better portrayed as traveling waves propagating through the cortex along anatomical pathways (6, 25, 57, 58). Moreover, different slow-oscillation patterns arise simultaneously from multiple origins throughout the cortex, creating complex local patterns rather than a single propagating wave (58, 59). Thus, although locally synchronized, concurrent slow oscillations in remote parts of the cortex may be out of phase. BG cells, even those that are closer in space, may receive convergent inputs from distinct, sometimes remote, regions of the cerebral cortex and thalamus (60). Representing the activity of cortical and thalamic areas whose oscillations may not be in phase, the slow oscillatory activity in two BG cells may not necessarily be synchronized. This consideration may help explain why the desynchronization observed here was not distance-related (Fig. 4*B*, *Inset*), as is the case for neural correlations (or the lack thereof) in the normal and parkinsonian pallidum (61, 62).

Spike–LFP Decoupling May Also Result from BG Convergent Anatomy. We have shown that contrary to the TC system, slow oscillation during SWS was weaker in the BG LFP, and that spiking in the BG (unlike TC) neurons was not phase-locked to the concurrent LFP. These results can be interpreted in the context of converging differential inputs to BG cells. By regarding the LFP as a sum of postsynaptic potentials of nearby neurons, we can compare the TC and BG networks in terms of their degree of shared input. In a population of neurons exhibiting higher degrees of shared input and similar anatomical geometry (like the cortical network, and unlike the BG), the barrage of postsynaptic potentials should be similar across cells. This may result in a more highly correlated LFP and greater slow-oscillation amplitudes (63), as we demonstrate for the TC network. Finally, this state of high input sharing should make spiking correlated between neurons and be coupled to the LFP (Fig. 4).

Therefore, we propose that just as for slow-oscillation desynchronization of the spiking activity, the weaker LFP slow oscillations and lack of spike–LFP coupling in the BG may stem from the convergent but still functionally segregated anatomy of this network. Further, the discordance between the prominent slow oscillation in BG spiking and its absence in the LFP may suggest that the BG LFP does not represent the major driving force behind cell spiking. BG LFP analysis is further complicated by volume conductance, as was shown in a recent paper which suggested that in the human STN, LFP recorded by monopolar electrodes is considerably affected by remote, presumably cortical, potentials (64).

In ketamine-anesthetized rats, single-neuron oscillations in the STN and GP were in-phase within the same nucleus (35). This discrepancy with the results presented here may be ascribed to the fact that deep anesthesia leads to more synchronized cortical oscillations, which may not allow for cross-region phase differences and cortical traveling waves. In this setting, the presumably convergent hardwiring of the cortico-BG anatomy is likely to preserve phase relationships rather than desynchronizing neuronal firing.

Slow Oscillation in Structures Receiving BG Output. Slow-oscillation synchronization in the cortex is thought to be crucial for long-range neural communication and effective memory consolidation during sleep (8). The BG example constitutes an exception to this putative association between oscillation and synchronization and raises the issue of the brain-wide advantages of desynchronization in slow oscillations. We suggest that the BG desynchronized output may play a role in brain-wide sleep physiology. The BG output structures (GPi and SNr) target the ventroanterior, ventrolateral, and intralaminar nuclei of the thalamus, which in turn innervate areas in the frontal cortex and widespread cortical areas, respectively. The BG funnel-like architecture may enable summation and convergence of TC input from vast cortical areas onto single BG output cells, thus possibly accounting for the increased fraction of cells exhibiting slow oscillations in the BG (Fig. 2*C*). Emerging from these results and considerations is the idea that the BG might supply a powerful returning and amplifying input of slow oscillation to cortical frontal regions.

An individual cortical slow wave can arise as a combination of patterns from independent origins that are active together (58, 59), and slow-oscillation hotspots usually occur in more anterior regions (25, 57). The BG slow-oscillation output back to cortical frontal areas may help to activate spontaneous potential hotspots, and their inherent lack of synchrony may allow these hotspots to be differentially active at any given time. In this sense, BG desynchrony might further the emergence of a scheme where the oscillation origins are widely dispersed and the cortical oscillations during natural sleep are not overly synchronized.

Concluding Remarks. Assessing the generalizability of our results and the possible contribution of BG slow-oscillation desynchronization in the context of brain-wide sleep physiology, we are restricted by some statistical limitations of the current design: first, the small number of animals used in this study, and second, the high interdependence of within-subject measures (i.e., neuronal activity in different brain regions within the same animal), holding the possibility for underlying confounding factors influencing the results. In future work, the first limitation might be resolved by the application of Bayesian statistical methods, which would make it possible to incorporate prior knowledge in the assessment of experimental data, especially when sample sizes are small (65).

To establish causal relationships between BG activity and sleep maintenance, future studies should utilize dissective methods aimed at silencing specific BG outputs (or abolishing their inherent desynchronized firing) and assess the resultant changes in vigilance. Such explorative efforts would benefit from the analysis of BG diseases such as Parkinson's disease, where extensive sleep alterations occur. Characterized by the underlying degeneration of the SNc dopaminergic neurons, an analysis of the specific alterations of neuronal activity in the parkinsonian brain (either in patients or in animal models) may shed light on the causal relations of BG activity and sleep maintenance, and suggest a new frame of clinical, circuit-based treatment for sleep disorders in Parkinson's disease.

In conclusion, we presented evidence for the existence of slow-oscillation desynchronization in the BG during SWS of nonhuman primates. We suggested that this desynchronization stems from the unique BG anatomy and that it may constitute a decorrelation mechanism for slow-wave generation in the cortex. A better understanding of BG sleep physiology and pathophysiology could pave the way for better treatments of sleep disorders that are highly common in Parkinson's and other BG-related diseases.

Materials and Methods

All experimental protocols were conducted in accordance with the National Institutes of Health *Guide for the Care and Use of Laboratory Animals* (66) and with the Hebrew University guidelines for the use and care of laboratory animals in research. The experiments were supervised by the Institutional Animal Care and Use Committee of the Faculty of Medicine, The Hebrew University. The Hebrew University is an Association for Assessment and Accreditation of Laboratory Animal Care internationally accredited institute.

Animals and Sleep Habituation. Data were obtained from two healthy, young adult, female vervet monkeys (*Chlorocebus aethiops sabaeus*; D and N)

weighing ~3.5 kg. Two key considerations prompted us to select nonhuman primates (over rodents or imaging human volunteers) as a model for this investigation. There are major differences between primates and rodents as regards sleep architecture (17), their functional brain network organization (67), and BG and frontal cortex anatomy and physiology (18, 19) but relative similarities between primates and humans. In addition, the fMRI blood oxygen level-dependent signal at current spatial and temporal resolutions does not reflect neuronal activity at the cellular level, and cannot be used to identify single-neuron and single-spike correlates of fundamental brain processes such as sleep.

The sleep recording routine was determined after a period of observation of the monkeys' sleep habits and schedules in the colony. The monkeys were habituated to sleeping in a primate chair, positioned in a dark, double-walled sound-attenuating room (IAC Acoustics). The primate chair restrained the monkeys' hand and body movements but otherwise allowed them to be in a position similar to their natural [sitting (20)] sleeping posture (Fig. S1*A*). Two to 3 mo before surgery, the monkeys were taken each evening (7 to 8 PM) into the room and left alone to sleep, with the lights off but under infrared video human supervision. Habituation proceeded gradually, and 2 wk before surgery the monkeys slept in the room the entire night (10 to 11 PM until 5 to 6 AM, 4 to 5 nights per wk). During the daytime and weekends the monkeys were housed in the monkey colony with their peers in a 2.5 × 3-m yard. The monkeys were also trained on a classic conditioning learning task which they performed in the evening, before sleep. During the day they were food-restricted, and were only fed during this ~1-h training and task performance. Supplementary food was given when the monkeys did not reach their daily caloric minimum.

Surgery and Magnetic Resonance Imaging. Following sleep habituation, the monkeys underwent a surgical procedure for the implantation of an MRI-compatible Cilux head holder (Crist Instrument) and a 27-mm (inner edge) square Cilux recording chamber (Alpha Omega Engineering) over the left hemisphere (22). The recording chamber was stereotaxically positioned 45° laterally in the coronal plane to cover most of the basal ganglia nuclei, frontal cortex, and ventral tier of the thalamus (68). Six titanium screws were screwed into the skull to allow for EEG recording (in both monkeys one of the EEG screws broke, so five were used). Finally, three titanium ground screws were placed in contact with the dura mater and connected to the chamber and head holder using a titanium wire. Recordings began after a postoperative recovery period of 5 to 7 d, during which an anatomical MRI scan (22) was performed to estimate the chamber coordinates of the neuronal targets.

Polysomnography and Sleep Staging. To determine the sleep stages throughout the entire night, the electroencephalogram, electrooculogram, and electromyogram were recorded and the eye state (open/closed) was monitored using continuous video recording. The scalp EEG was recorded from five locations (three in the left hemisphere and two in the right): frontal (F_3), central (C_1, C_4), and posterior-occipital derivations (PO_3 and PO_4). EEG locations are cited with respect to the modified combinatorial nomenclature for the EEG-positioning 10–20 system, standardized by the American Electroencephalographic Society (69). EOG was recorded from each eye separately using disposable paired pregelled surface electrodes (Rhythmlink International). EEG and EOG channels were referenced to a common ground: two titanium epidural ground screws that were interconnected and positioned at P_5 and FC_6. EMG was recorded using disposable paired (bipolar recording) subdermal needle electrodes (Rhythmlink International), inserted into the right trapezius muscle. This location was selected after screening of several axial muscles, as it allowed for a high-amplitude signal and good discrimination between the tonic muscle activity during different sleep stages (Fig. S2).

All polysomnographic measures were sampled at 2,750 Hz. EEG and EOG were digitally bandpass-filtered in the range of 0.1 to 35 Hz (Butterworth filter, stopband at 0 to 0.05 Hz, 40 to 1,375 Hz. Minimal passband to stopband attenuation, 10 dB. Forward–backward filtering was used to minimize phase distortions. Filter specifications were the same for all filters, so hereafter filters are specified only by passband and stopband ranges). EMG was bandpass-filtered in the range of 10 to 100 Hz (stopband at 0 to 5 Hz, 120 to 1,375 Hz). Positioning of electrodes, sampling, and filtration followed the recommendations of the American Association of Sleep Medicine (AASM) *Manual for the Scoring of Sleep and Associated Events* (70). The monkeys were digitally video-recorded at 50 frames per s using an infrared camera (640 × 480 pixels; NorPix) to assist sleep staging by detection of the eye-open/closed state.

Sleep staging was done using a semiautomatic staging algorithm (custom software) that used clustering of 10-s nonoverlapping epochs, based on three features: (*i*) the average high/low EEG power ratio across all contacts, where the average power at 15 to 25 Hz (related to waking) was divided by the average power at 0.1 to 7 Hz (related to sleep); (*ii*) root mean square (RMS) of the EMG signal; and (*iii*) eye-open fraction. Eye states were automatically determined based on the number of dark pixels in the eye area. Every 10-s epoch was represented as a point in three-dimensional feature space (71), usually forming three clusters: for wakefulness (high EMG RMS, increased EEG high/low ratio, eye-open fraction close to 1), NREM (low EMG RMS, decreased EEG high/low ratio, eye-open fraction close to 0), and REM (very low EMG RMS, increased EEG high/low ratio, eye-open fraction close to 0). The three clusters were delineated manually, leaving outlier points unclassified (Fig. 1*A*). Before semiautomatic clustering, 10% of the night epochs were scored manually by a trained expert (A.D.M.-K.; provided they contained all sleep stages. If not, manual staging proceeded until epochs from all stages were encountered). The staging results provided by the semiautomatic algorithm were accepted for further analysis only if they matched the expert staging in more than 85% of the tested epochs. In the few cases where adequate agreement was not achieved, EEG high- and low-frequency ranges were modified to allow for better discrimination.

NREM epochs were divided into SWS and N1/2 epochs: EEG traces were 0.1- to 2-Hz bandpass-filtered (stopband: 0 to 0.05 Hz, 2.5 to 1,375 Hz). In each 10-s epoch, slow-oscillation segments were defined as segments in which the instantaneous amplitude of the 0.1- to 2-Hz oscillation (calculated using the Hilbert transform of the filtered signal) exceeded a 40-μV threshold in the frontal or central EEG derivations. If the total duration of slow-oscillation segments in a 10-s epoch exceeded 20% of the epoch length, this epoch was staged as SWS. Otherwise, it was staged as N1/2. This differentiation is consistent with the AASM criteria. The only exceptions were our broader definition of the slow-oscillation range (0.1 to 2 Hz instead of 0.5 to 2 Hz, which was utilized to make sure no lower slow-oscillation range power was lost), the minimal voltage threshold for defining N3 (40 μV instead of 75 μV, consistent with the midskull location of our reference vs. mastoid reference), and our additional use of the central EEG electrodes instead of only frontal ones. Therefore, we termed the epochs staged in this way "SWS" rather than "N3." Analysis of a subset of the data staged using N3 criteria returned similar results.

Electrophysiological Recordings and Data Collection. Recording sessions followed the sleep habituation routine (4 to 6 nights a week, 10 to 11 PM to 5 to 6 AM). The monkeys' heads were immobilized with a head holder and eight glass-coated tungsten microelectrodes (confined by an ~1.7-mm internal diameter guide, impedance 0.4 to 1 MΩ at 1 kHz; Alpha Omega Engineering) were advanced separately (Electrode Positioning System; Alpha Omega Engineering) by two experimenters toward the targeted structures. Electrical activity was amplified with a gain of 20, filtered using a hardware Butterworth filter (highpass: 0.075 Hz, two poles; lowpass: 10 kHz, three poles), and sampled at 44 kHz by a 16-bit (±1.25-V input range) analog/digital converter. Spiking activity was sorted online using a template matching algorithm (SnR; Alpha Omega Engineering). BG and thalamocortical neuronal assemblies were identified according to their stereotaxic coordinates, based on MRI and primate atlas data (68) and real-time assessment of their electrophysiological features (22).

Preparation of Online-Sorted Units for Offline Analysis. Neuronal stability periods were first defined online, based on the technical quality of the unit isolation and stability of recording. Offline single-neuron and pair analyses were conducted only for unquestionably identified, stably held, and well-isolated neurons (72). Neurons exhibiting a stable firing rate for ≥3 min (73) and an average isolation score ≥0.85 (≥0.8 for MSNs and thalamus neurons; ≥0.7 for STN and cortex neurons) were further analyzed. The adjustment of the inclusion criteria for MSNs, thalamus, cortex, and STN neurons was prompted by their relatively dense cellular arrangement, which makes isolation difficult. Analysis of the subset of those neurons displaying an isolation score ≥0.85 and a stable firing rate for ≥10 min yielded similar results to those reported here. The average isolation score for all of the cells included in all of the analyses was 0.93, and the mean recording time was 43 min (Table S1). The average isolation score for neuron pairs was calculated as the mean score of all neurons in all pairs.

Firing Rate, Firing Pattern, and Power Spectrum Analysis. Each neuronal unit's recording time was segmented into 10-s epochs corresponding to the sleep staging epochs. For GPe, GPi, and SNr cells, pauses were detected using the modified surprise method (74). The spike count was measured for all 5-ms nonoverlapping bins, and the 10-s epoch mean was subtracted to eliminate the DC (direct current, 0 Hz) component. The per-epoch firing rate power spectrum was obtained [Hamming window, NFFT (no. of fast Fourier transform points): 2,048; frequency resolution: 0.098 Hz. Different bin lengths, window functions, and numbers of FFT points yielded similar results]. The relative power at each frequency was then calculated by division of the

entire spectrum by the overall power in the range of 0.1 to 35 Hz. The mean slow-oscillation frequency (during SWS epochs) was calculated as the average instantaneous frequency of the epoch (obtained using the Hilbert transform after 0.1- to 2-Hz filtering).

To verify that our results were not confounded by the differences between the average firing rates of the different neuronal species (26), we calculated the power spectra of the spike-pruned signals for all of the BG high-frequency discharge structures. Spikes were randomly pruned to arrive at a firing rate of four or two spikes/s (mean firing rate of the cortex and MSN neurons during SWS, respectively). The power spectrum of the resulting signal was calculated as described above. Random pruning and power spectra calculations were repeated 10 times and then averaged. A low-to-high firing rate power ratio was calculated for every neuron and sleep stage by dividing the mean relative power at 0.1 to 2 Hz by the mean relative power at 9 to 15 Hz. A cell was considered to exhibit slow oscillations if its LHPR during SWS was significantly higher (Wilcoxon signed-rank test, $P = 0.05$) than the median of the distribution of LHPRs for REM sleep and wakefulness combined, and significantly higher than 1. If a given cell was only recorded during SWS, its SWS LHPR only needed to be higher than 1.

We also conducted a similar spectral analysis of the local field potential recorded in the vicinity of each of the analyzed neurons. The raw signal (hardware filtered between 0.075 Hz and 10 kHz, and sampled at 44 kHz) was digitally bandpass-filtered (0.1 to 35 Hz; stopband: 0 to 0.05 Hz, 40 to 22,000 Hz) and downsampled to 1,375 Hz.

Cross-Correlation Analysis. Pairs for cross-correlation analysis were recorded from the same neuronal assembly but from two different electrodes to overcome the shadowing effect of units recorded by the same electrode (75). A 3,000-ms segment around each of the spikes of the (randomly assigned) trigger neuron was defined and binned to 5-ms bins. The number of spikes fired by the other, reference, neuron in each of these bins was averaged across trigger neuron spikes and divided by the bin length and the number of trigger spikes to obtain a conditional firing rate in spikes/s. Trigger neuron spikes that were less than 1,500 ms away from the beginning or end of an epoch were not considered for analysis. Cross-correlograms were smoothed using a 10-ms Gaussian kernel (MSN traces were smoothed using a 30-ms kernel to compensate for the slow discharge rate of the MSNs). The area under the curve of the cross-correlogram was calculated using trapezoidal numeric integration for the interval of 1,500 ms around the trigger spike. The zero point for integration was set as the average activity in the first and last 500-ms intervals of the 3,000-ms segment.

Analysis of Phase Relationships Between Slow-Oscillation Waves. Neuron pairs where both neurons exhibited slow oscillatory activity, were recorded during an SWS epoch, and also exhibited 0.1- to 2-Hz power greater than a predefined threshold, were analyzed for their phase relationships. For the randomly selected trigger and reference neuron, a firing rate vector was obtained as previously described. The firing rate vector was filtered in the slow-oscillation range, and slow-oscillation peaks were found. Peaks had to maintain a minimal 350-ms distance, and have a minimal instantaneous amplitude (defined as the 50th percentile of the 0.1- to 2-Hz instantaneous amplitude distribution, for all of the neuron's NREM periods). For each of the trigger neuron's slow-oscillation peaks, the instantaneous phase of the reference neuron was found. To merit further analysis, the pair of neurons had to meet two additional criteria: The instantaneous slow-oscillation amplitude of the reference neuron in the sample corresponding to the trigger neuron peak had to be the minimal amplitude stated for the trigger neuron, and the difference between the average oscillation frequencies of both neurons (evaluated over one period around the peak point) had to be less than 0.3 Hz. The phase-lock index (range 0 to 1) was calculated for the acquired phase differences. Different amplitude thresholds and oscillation frequency differences yielded similar results.

To assess the similarity between concurrent oscillations, we also calculated Pearson's correlation between full slow-oscillation waveforms for the simultaneously recorded cells. The correlation was calculated between segments of one period around each of the peaks of the trigger neuron, and the corresponding segments for the reference neurons. To correct for the different firing rates of each neuron, the segments were normalized by subtraction of their mean and division by their respective SDs (z-score normalization). Wave-to-wave correlation histograms were smoothed by an 8-point Gaussian kernel to allow for better visualization.

To explore the coupling between a neuron's spiking activity and the slow oscillation of the LFP recorded in its vicinity, we calculated the instantaneous phase of the filtered LFP (passband: 0.1 to 2 Hz; stopband: 0 to 0.05 Hz, 2.5 to 22,000 Hz. Phases ranged from $-\pi$ to π, and were binned to 1,000 2π/1,000 rad-sized bins) for each spike timing. Only spikes that were concurrent with an LFP slow oscillation with an instantaneous amplitude greater than a predefined threshold (the 50th percentile of the slow-oscillation instantaneous amplitude distribution in the original LFP) were further analyzed. Using a neuron-specific threshold allowed us to correct for interstructure and interneuron differences and to only take traces of activity that showed genuine slow oscillation into consideration. The spike count corresponding to each phase bin of the trigger neuron was used to compute the single-neuron spike to the LFP phase-lock index. Spikes in the range of 3,000 ms around each oscillation trough were summed and averaged across waves to obtain a delay map of the neuron's spiking activity in relation to the LFP slow-oscillation troughs. The same analysis, building on the LFP from a trigger neuron and spikes from a reference neuron, yielded similar results.

The distance between simultaneously recorded neurons was assessed using the Euclidean distance between the estimated locations of the microelectrode tips. The distance between the middle of the shafts of each of the microelectrodes was assessed by a digitized high-resolution image of the shafts, and the depth of each recording site relative to the depth in which the brain was penetrated was estimated using the 1-μm-resolution electrode-positioning system.

Statistics. Analysis was conducted identically on all neuronal assemblies. The data from the two monkeys were pooled since no significant differences were detected between them. A threshold of 0.05 was used to establish statistical significance. ANOVA and Student's *t* test were only used when neither of the assumptions of ANOVA was violated, namely an underlying normal distribution and homogeneity of the variance. Thus, ANOVA was used when (*i*) samples were large and represented the sum of random variables; that is, they distributed normally according to the central limit theorem. Nevertheless, it is worth noting that ANOVA is usually robust to violations of the normality assumption (76). (*ii*) All groups were variance-homogeneous. When one of the two ANOVA assumptions was not met, nonparametric statistical tests were used. The Bonferroni correction was used when the number of comparisons was small (<15), and the false discovery rate (FDR) correction (Benjamini–Hochberg procedure) was used otherwise. Significant *P* values are reported postcorrection. All statistical tests were two-tailed. Analyses and statistical computations were performed using Matlab 2013b (MathWorks) and SPSS 24 (IBM). Data and code are available from the Basal Ganglia data repository (basalganglia.huji.ac.il/links.htm).

ACKNOWLEDGMENTS. We thank Dr. Yaron Dagan and Dr. Tamar Ravins-Yaish for assistance with animal care, and Dr. Atira Bick and Dr. Adi Payis for assistance with MRI scanning. We thank Anatoly Shapochnikov, Dr. Hila Gabbay, Dr. Sharon Freeman, Dr. Uri Werner-Reiss, and Esther Singer for general assistance. We thank Dr. Marc Deffains for his assistance in neuronal recordings, and Dr. Yuval Nir for his assistance in planning the experiments and the analysis of the results. This work was supported by grants from the European Research Council, Israel Science Foundation, and Rosetrees Trust (to H.B.).

1. Nir Y, Massimini M, Boly M, Tononi G (2013) Sleep and consciousness. *Neuroimaging of Consciousness*, eds Cavanna AE, Nani A, Blumenfeld H, Laureys S (Springer, Berlin), pp 133–182.
2. Timofeev I, Grenier F, Steriade M (2001) Disfacilitation and active inhibition in the neocortex during the natural sleep-wake cycle: An intracellular study. *Proc Natl Acad Sci USA* 98:1924–1929.
3. Destexhe A, Contreras D, Steriade M (1999) Spatiotemporal analysis of local field potentials and unit discharges in cat cerebral cortex during natural wake and sleep states. *J Neurosci* 19:4595–4608.
4. Steriade M, Contreras D, Curró Dossi R, Nuñez A (1993) The slow (< 1 Hz) oscillation in reticular thalamic and thalamocortical neurons: Scenario of sleep rhythm generation in interacting thalamic and neocortical networks. *J Neurosci* 13:3284–3299.
5. Wolansky T, Clement EA, Peters SR, Palczak MA, Dickson CT (2006) Hippocampal slow oscillation: A novel EEG state and its coordination with ongoing neocortical activity. *J Neurosci* 26:6213–6229.
6. Nir Y, et al. (2011) Regional slow waves and spindles in human sleep. *Neuron* 70: 153–169.
7. Eschenko O, Magri C, Panzeri S, Sara SJ (2012) Noradrenergic neurons of the locus coeruleus are phase locked to cortical up-down states during sleep. *Cereb Cortex* 22: 426–435.
8. Mölle M, Born J (2011) Slow oscillations orchestrating fast oscillations and memory consolidation. *Slow Brain Oscillations of Sleep, Resting State and Vigilance*, eds Van Someren EJW, Van Der Werf YD, Roelfsema PR, Mansvelder HD, Lopes Da Silva FH (Elsevier, Amsterdam), pp 93–110.

9. Volgushev M, Chauvette S, Mukovski M, Timofeev I (2006) Precise long-range synchronization of activity and silence in neocortical neurons during slow-wave sleep. *J Neurosci* 26:5665–5672.
10. Kincaid AE, Zheng T, Wilson CJ (1998) Connectivity and convergence of single corticostriatal axons. *J Neurosci* 18:4722–4731.
11. Smith Y, et al. (2014) The thalamostriatal system in normal and diseased states. *Front Syst Neurosci* 8:5.
12. Kolomiets BP, et al. (2001) Segregation and convergence of information flow through the cortico-subthalamic pathways. *J Neurosci* 21:5764–5772.
13. Daw ND, Niv Y, Dayan P (2006) Actions, policies, values, and the basal ganglia. *Recent Breakthroughs in Basal Ganglia Research*, ed Bezard E (Nova Science, Hauppauge, NY), pp 91–106.
14. Graybiel AM (2008) Habits, rituals, and the evaluative brain. *Annu Rev Neurosci* 31: 359–387.
15. Qiu MH, Vetrivelan R, Fuller PM, Lu J (2010) Basal ganglia control of sleep-wake behavior and cortical activation. *Eur J Neurosci* 31:499–507.
16. Eban-Rothschild A, Rothschild G, Giardino WJ, Jones JR, de Lecea L (2016) VTA dopaminergic neurons regulate ethologically relevant sleep-wake behaviors. *Nat Neurosci* 19:1356–1366.
17. Toth LA, Bhargava P (2013) Animal models of sleep disorders. *Comp Med* 63:91–104.
18. Hardman CD, et al. (2002) Comparison of the basal ganglia in rats, marmosets, macaques, baboons, and humans: Volume and neuronal number for the output, internal relay, and striatal modulating nuclei. *J Comp Neurol* 445:238–255.
19. Benhamou L, Bronfeld M, Bar-Gad I, Cohen D (2012) Globus pallidus external segment neuron classification in freely moving rats: A comparison to primates. *PLoS One* 7: e45421.
20. Albert A, Savini T, Huynen MC (2011) Sleeping site selection and presleep behavior in wild pigtailed macaques. *Am J Primatol* 73:1222–1230.
21. Hsieh KC, Robinson EL, Fuller CA (2008) Sleep architecture in unrestrained rhesus monkeys (*Macaca mulatta*) synchronized to 24-hour light-dark cycles. *Sleep* 31: 1239–1250.
22. Deffains M, et al. (2016) Subthalamic, not striatal, activity correlates with basal ganglia downstream activity in normal and parkinsonian monkeys. *Elife* 5:e16443.
23. Deister CA, Dodla R, Barraza D, Kita H, Wilson CJ (2013) Firing rate and pattern heterogeneity in the globus pallidus arise from a single neuronal population. *J Neurophysiol* 109:497–506.
24. DeLong MR (1971) Activity of pallidal neurons during movement. *J Neurophysiol* 34: 414–427.
25. Massimini M, Huber R, Ferrarelli F, Hill S, Tononi G (2004) The sleep slow oscillation as a traveling wave. *J Neurosci* 24:6862–6870.
26. Matzner A, Bar-Gad I (2015) Quantifying spike train oscillations: Biases, distortions and solutions. *PLoS Comput Biol* 11:e1004252.
27. Chauvette S, Volgushev M, Timofeev I (2010) Origin of active states in local neocortical networks during slow sleep oscillation. *Cereb Cortex* 20:2660–2674.
28. Cole SR, et al. (2017) Nonsinusoidal beta oscillations reflect cortical pathophysiology in Parkinson's disease. *J Neurosci* 37:4830–4840.
29. DeLong MR (1969) Activity of pallidal neurons in the monkey during movement and sleep. *Physiologist* 12:207.
30. Adler A, et al. (2010) Neurons in both pallidal segments change their firing properties similarly prior to closure of the eyes. *J Neurophysiol* 103:346–359.
31. Urbain N, et al. (2000) Unrelated course of subthalamic nucleus and globus pallidus neuronal activities across vigilance states in the rat. *Eur J Neurosci* 12:3361–3374.
32. Mahon S, et al. (2006) Distinct patterns of striatal medium spiny neuron activity during the natural sleep-wake cycle. *J Neurosci* 26:12587–12595.
33. Stefani A, et al. (2006) Spontaneous sleep modulates the firing pattern of parkinsonian subthalamic nucleus. *Exp Brain Res* 168:277–280.
34. Stern EA, Kincaid AE, Wilson CJ (1997) Spontaneous subthreshold membrane potential fluctuations and action potential variability of rat corticostriatal and striatal neurons in vivo. *J Neurophysiol* 77:1697–1715.
35. Magill PJ, Bolam JP, Bevan MD (2000) Relationship of activity in the subthalamic nucleus-globus pallidus network to cortical electroencephalogram. *J Neurosci* 20: 820–833.
36. Kasanetz F, Riquelme LA, Murer MG (2002) Disruption of the two-state membrane potential of striatal neurones during cortical desynchronisation in anaesthetised rats. *J Physiol* 543:577–589.
37. Goldberg JA, Kats SS, Jaeger D (2003) Globus pallidus discharge is coincident with striatal activity during global slow wave activity in the rat. *J Neurosci* 23:10058–10063.
38. Saper CB, Scammell TE, Lu J (2005) Hypothalamic regulation of sleep and circadian rhythms. *Nature* 437:1257–1263.
39. Charara A, Parent A (1994) Brainstem dopaminergic, cholinergic and serotoninergic afferents to the pallidum in the squirrel monkey. *Brain Res* 640:155–170.
40. Dautan D, et al. (2014) A major external source of cholinergic innervation of the striatum and nucleus accumbens originates in the brainstem. *J Neurosci* 34: 4509–4518.
41. Trulson ME, Preussler DW, Howell GA (1981) Activity of substantia nigra units across the sleep-waking cycle in freely moving cats. *Neurosci Lett* 26:183–188.
42. Steinfels GF, Heym J, Strecker RE, Jacobs BL (1983) Behavioral correlates of dopaminergic unit activity in freely moving cats. *Brain Res* 258:217–228.
43. Nishino S, Mao J, Sampathkumaran R, Shelton J (1998) Increased dopaminergic transmission mediates the wake-promoting effects of CNS stimulants. *Sleep Res Online* 1:49–61.
44. Qiu M-H, Yao Q-L, Vetrivelan R, Chen MC, Lu J (2016) Nigrostriatal dopamine acting on globus pallidus regulates sleep. *Cereb Cortex* 26:1430–1439.
45. Belaid H, et al. (2014) Sleep disorders in parkinsonian macaques: Effects of L-dopa treatment and pedunculopontine nucleus lesion. *J Neurosci* 34:9124–9133.
46. Jennings KA, Platt NJ, Cragg SJ (2015) The impact of a parkinsonian lesion on dynamic striatal dopamine transmission depends on nicotinic receptor activation. *Neurobiol Dis* 82:262–268.
47. Nini A, Feingold A, Slovin H, Bergman H (1995) Neurons in the globus pallidus do not show correlated activity in the normal monkey, but phase-locked oscillations appear in the MPTP model of parkinsonism. *J Neurophysiol* 74:1800–1805.
48. Fukai T, Tanaka S (1997) A simple neural network exhibiting selective activation of neuronal ensembles: From winner-take-all to winners-share-all. *Neural Comput* 9: 77–97.
49. Wilson CJ (2013) Active decorrelation in the basal ganglia. *Neuroscience* 250:467–482.
50. Alexander GE, DeLong MR, Strick PL (1986) Parallel organization of functionally segregated circuits linking basal ganglia and cortex. *Annu Rev Neurosci* 9:357–381.
51. Parent M, Parent A (2006) Relationship between axonal collateralization and neuronal degeneration in basal ganglia. *Parkinson's Disease and Related Disorders*, eds Riederer P, Reichmann H, Youdim MBH, Gerlach M (Springer, Vienna), pp 85–88.
52. Plenz D (2003) When inhibition goes incognito: Feedback interaction between spiny projection neurons in striatal function. *Trends Neurosci* 26:436–443.
53. Joshua M, et al. (2009) Synchronization of midbrain dopaminergic neurons is enhanced by rewarding events. *Neuron* 62:695–704.
54. Oorschot DE (1996) Total number of neurons in the neostriatal, pallidal, subthalamic, and substantia nigral nuclei of the rat basal ganglia: A stereological study using the cavalieri and optical disector methods. *J Comp Neurol* 366:580–599.
55. Percheron G, Yelnik J, François C (1984) A Golgi analysis of the primate globus pallidus. III. Spatial organization of the striato-pallidal complex. *J Comp Neurol* 227: 214–227.
56. Hazrati L-N, Parent A (1992) Convergence of subthalamic and striatal efferents at pallidal level in primates: An anterograde double-labeling study with biocytin and PHA-L. *Brain Res* 569:336–340.
57. Menicucci D, et al. (2009) Functional structure of spontaneous sleep slow oscillation activity in humans. *PLoS One* 4:e7601.
58. Murphy M, et al. (2009) Source modeling sleep slow waves. *Proc Natl Acad Sci USA* 106:1608–1613.
59. Botella-Soler V, Valderrama M, Crépon B, Navarro V, Le Van Quyen M (2012) Large-scale cortical dynamics of sleep slow waves. *PLoS One* 7:e30757.
60. Choi EY, Tanimura Y, Vage PR, Yates EH, Haber SN (2017) Convergence of prefrontal and parietal anatomical projections in a connectional hub in the striatum. *Neuroimage* 146:821–832.
61. Bar-Gad I, Heimer G, Ritov Y, Bergman H (2003) Functional correlations between neighboring neurons in the primate globus pallidus are weak or nonexistent. *J Neurosci* 23:4012–4016.
62. Mitelman R, et al. (2011) Neighboring pallidal neurons do not exhibit more synchronous oscillations than remote ones in the MPTP primate model of Parkinson's disease. *Front Syst Neurosci* 5:54.
63. Buzsáki G, Anastassiou CA, Koch C (2012) The origin of extracellular fields and currents—EEG, ECoG, LFP and spikes. *Nat Rev Neurosci* 13:407–420.
64. Marmor O, et al. (2017) Local vs. volume conductance activity of field potentials in the human subthalamic nucleus. *J Neurophysiol* 117:2140–2151.
65. van de Schoot R, et al. (2014) A gentle introduction to Bayesian analysis: Applications to developmental research. *Child Dev* 85:842–860.
66. National Research Council (2011) *Guide for the Care and Use of Laboratory Animals* (Natl Acad Press, Washington, DC), 8th Ed.
67. Hutchison RM, Everling S (2012) Monkey in the middle: Why non-human primates are needed to bridge the gap in resting-state investigations. *Front Neuroanat* 6:29.
68. Martin RF, Bowden DM (2000) *Primate Brain Maps: Structure of the Macaque Brain* (Elsevier, Amsterdam).
69. Sharbrough F, et al. (1991) American Electroencephalographic Society guidelines for standard electrode position nomenclature. *J Clin Neurophysiol* 8:200–202.
70. Iber C, Ancoli-Israel S, Chesson AL, Quan SF (2007) *The AASM Manual for the Scoring of Sleep and Associated Events: Rules, Terminology and Technical Specifications* (Am Assoc Sleep Med, Westchester, IL).
71. Nir Y, Vyazovskiy VV, Cirelli C, Banks MI, Tononi G (2015) Auditory responses and stimulus-specific adaptation in rat auditory cortex are preserved across NREM and REM sleep. *Cereb Cortex* 25:1362–1378.
72. Joshua M, Elias S, Levine O, Bergman H (2007) Quantifying the isolation quality of extracellularly recorded action potentials. *J Neurosci Methods* 163:267–282.
73. Gourévitch B, Eggermont JJ (2007) A simple indicator of nonstationarity of firing rate in spike trains. *J Neurosci Methods* 163:181–187.
74. Elias S, et al. (2007) Statistical properties of pauses of the high-frequency discharge neurons in the external segment of the globus pallidus. *J Neurosci* 27:2525–2538.
75. Bar-Gad I, Ritov Y, Vaadia E, Bergman H (2001) Failure in identification of overlapping spikes from multiple neuron activity causes artificial correlations. *J Neurosci Methods* 107:1–13.
76. Schmider E, Ziegler M, Danay E, Beyer L, Bühner M (2010) Is it really robust? Reinvestigating the robustness of ANOVA against violations of the normal distribution assumption. *Eur J Res Methods Behav Soc Sci* 6:147–151.